Syntheses, crystal structures, thermal stabilities, luminescence and magnetism of two 3D pillared metal phosphonates†‡

Ruibiao Fu,* Shengmin Hu and Xintao Wu*

Received 16th April 2009, Accepted 18th September 2009
First published as an Advance Article on the web 14th October 2009
DOI: 10.1039/b907619k

Two pillared metal phosphonates: $[Mn_3(4,4'\text{-bipy})(L)_2]\cdot(4,4'\text{-bipy})_{0.5}$ (**1**) and $[Co_3(4,4'\text{-bipy})(H_2O)_2(L)_2]\cdot(4,4'\text{-bipy})_{0.5}$ (**2**) (L = $O_3PCH(OH)CO_2$), have been synthesized hydrothermally, and characterized by single-crystal X-ray diffraction along with powder XRD, EA, IR and TGA. In compounds **1–2**, Mn(II) and Co(II) ions are in octahedron coordination geometries and bridged by 2-hydroxyl(phosphono)acetate through -OH, -COO and -PO_3 groups into a hybrid layer. The layers are further pillared by the coordinated 4,4′-bipy into a 3D neutral framework possessing 1D parallelogram-shaped channels with approximate sizes 9×11 Å^2, which are occupied by the isolated 4,4′-bipy. Solid **1** is thermally stable up to 300 °C under an air atmosphere and displays a purple-blue luminescence. The results of magnetic measurement indicate solid **1** is a metamagnet.

Introduction

Metal phosphonates are a new class of hybrid materials known for their structural diversities and potential or practical applications as Langmuir-Blodgett Films (LB), meso/microporous materials, ion-exchangers, small molecular sensors, catalysts, non-linear optics, and so on.[1] After the pioneering work of Clearfield, the design and synthesis of new metal phosphonates with interesting structures and attractive properties have flourished over the last five years.[2] Most metal monophosphonates (M/RPO_3) are 2D layered structures and useful in the area of intercalation chemistry.[3] While metal diphosphonates ($M/O_3P\text{-}R\text{-}PO_3$) usually exhibit 3D pillared open-frameworks and have been exploited as meso/microporous materials. The 3D pillared structures can be fine-tuned *via* modifying the lengths and shapes of the organic units.[4] Enantiopure organophosphonic acids are introduced as asymmetric units to obtain homochiral porous lanthanide phosphonates with 1D triple-strand helical chains and selective adsorption capacities for N_2, H_2O, and CH_3OH molecules, $Zn_2[(S)\text{-}O_3PCH_2NHC_4H_7CO_2]_2$ with helical channels as well as homochiral zinc phosphonates.[5] Ferrocenylphosphonic acid has been selected as a ligand to prepare a mixed 1D–2D inorganic polymeric zinc ferrocenylphosphonate with electroactivity and two cage-type tetranuclear metal clusters with strong third-order nonlinear optical (NLO) self-focusing effects.[6] Many metal phosphonate clusters like manganese, iron and cobalt, display intriguing structures and magnetic properties.[7] One important research direction is to introduce additional functional groups such as NH_2, OH, COOH, crown ether, pyridyl, and benzimidazole into phosphonate ligands. Such ligands exhibit various coordination modes, resulting in many interesting solids, including $M_x[Fe(O_2CCH_2)_2NCH_2PO_3]_6\cdot nH_2O$ (M = Na, K, Rb) with a maple leaf lattice, nickel N,N′-piperazinebis(methylenephosphonate) possessing large pores greater than *ca.* 10 Å (free diameter), copper macrocyclic leaflets, and lanthanide phosphonates with blue, red and near IR luminescence.[8-12] In this regard, 2-hydroxyl(phosphono)acetic acid with three functional groups (-PO_3H_2, -CO_2H and -OH) and bright blue-green luminescence has been successfully explored to synthesize four hybrid layers $M(HO_3PCH(OH)CO_2)(H_2O)_2$ (M = Mn, Fe, Co, Zn) with antiferromagnetic property, four 3D heterometal phosphonates $NaM(O_3PCH(OH)CO_2)$ (M = Mn, Fe, Co, Zn) which display the irreversible transformation of luminescent color, as well as a new 3D open-framework $(NH_4)Zn(O_3PCH(OH)CO_2)$ featuring nonlinear optical activity and high thermal stability.[13] The other interesting research direction is to introduce secondary ligands like 1,10-phenanthroline, 2,2′-bipyridine, 4,4′-bipyridine and tetra-2-pyridylpyrazine into metal phosphonates to prepare novel hybrid materials with polynuclear clusters, chains, layers and 3D open-frameworks.[14-15] Inspired by the above results, 4,4′-bipyridine has been selected as a secondary ligand to expand the framework of metal 2-hydroxyl(phosphono)acetate. In this paper, we report the synthesis, crystal structures, thermal stabilities, luminescence and magnetism of two 3D pillared metal phosphonates: $[Mn_3(4,4'\text{-bipy})(L)_2]\cdot(4,4'\text{-bipy})_{0.5}$ (**1**) and $[Co_3(4,4'\text{-bipy})(H_2O)_2(L)_2]\cdot(4,4'\text{-bipy})_{0.5}$ (**2**) (L= $O_3PCH(OH)CO_2$).

Experimental

Materials and instrumentation

2-Hydroxyl(phosphono)acetic acid solution was obtained from Changzhou City Jianghai Chemical Factory as a water treatment agent (*wt.*% = 48.0%). All other chemicals were obtained from commercial sources without further purification. Compounds **1–2** were synthesized in 25 mL Teflon™-lined stainless steel

State Key Laboratory of Structural Chemistry, Fujian Institute of Research on the Structure of Matter, Chinese Academy of Science Fuzhou, Fujian, 350002, China. E-mail: wxt@fjirsm.ac.cn; Fax: +86-591-83794946; Tel: +86-591-83792837

† Electronic supplementary information (ESI) available: IR and luminescent emission spectra, TGA curves, powder XRD patterns, temperature dependence of the zero field-cooled magnetic susceptibility, as well as *M versus H* curves. CCDC reference numbers 727228 and 727229 for compounds **1** and **2**, respectively. For ESI and crystallographic data in CIF or other electronic format see DOI: 10.1039/b907619k

‡ Dedicated to Prof. Xin-Tao Wu on the occasion of his 70th birthday.

vessels under autogenous pressure. The reactants were stirred homogeneously before heating. Elemental analyses were carried out with a Vario EL III element analyzer. Infrared spectra were obtained on a Nicolet Magna 750 FT-IR spectrometer. Fluorescent properties of solid **1** were performed with FLS920 and LifeSpec-ps under room temperature. Thermogravimetric analysis (TGA) was performed on a NETZSCH STA449C at a heating rate of 10 °C min^{-1} from room temperature to 1000 °C under air and nitrogen gas flow for solids **1** and **2**, respectively. Powder XRD patterns were acquired on a DMAX-2500 diffractometer and an XPERT-PRO diffractometer using Cu Kα radiation at ambient environment.

Synthesis

$[Mn_3(4,4'\text{-bipy})(O_3PCH(OH)CO_2)_2]\cdot(4,4'\text{-bipy})_{0.5}$ (1). A mixture of $Mn(CH_3COO)_2\cdot 4H_2O$ (0.2450 g, 0.9996 mmol), 4,4′-bipyridine (0.1681 g, 1.076 mmol), $(H_2O_3P)CH(OH)(CO_2H)$ solution (0.4 mL, 1.6 mmol), tris(2-hydroxyethyl)amine 0.1 mL and 10.0 mL H_2O was heated at 180 °C for 120 h. After slow cooling to room temperature, the pH value of this reaction mixture was 4.34. The final mixture was rinsed with distilled water under ultrasonication many times to obtain pure colorless crystals as a homogenous phase based on the powder XRD patterns. Yield: 0.1185 g (50%). Anal. Calc. for $C_{19}H_{16}N_3O_{12}P_2Mn_3$: C 32.36, H 2.29, N 5.96%. Found: C 31.90, H 2.64, N 5.64%. IR (KBr pellet, cm^{-1}): 2970w ($\nu_{C\text{-}H}$), 2735w, 2667w, 2611w, 1587vs ($\nu_{as CO}$), 1533m, 1491w, 1416w, 1381m, 1254m, 1223 m, 1167s ($\nu_{P=O}$), 1128s ($\nu_{P\text{-}O}$), 1047s ($\nu_{P\text{-}O}$), 972 ($\nu_{P\text{-}O}$), 852w, 806m, 798m, 758m, 690m, 633 m, 607m, 501m.

$[Co_3(4,4'\text{-bipy})(H_2O)_2(O_3PCH(OH)CO_2)_2]\cdot(4,4'\text{-bipy})_{0.5}$ (2). A mixture of $Co(CH_3COO)_2\cdot 4H_2O$ (0.1129 g, 0.4533 mmol), 4,4′-bipyridine (0.1685 g, 1.079 mmol), $(H_2O_3P)CH(OH)(CO_2H)$ solution (0.2 mL, 0.8 mmol), S-(+)-2-$C_5H_{12}N_2$ (0.0294 g, 0.2934 mmol) and 10.0 mL H_2O was heated at 180 °C for 144 h. After slow cooling to room temperature, the pH value of this reaction mixture was 4.43. The final mixture was rinsed with distilled water under ultrasonication many times to obtain pure red crystals as a homogenous phase based on the powder XRD patterns. Yield: 0.0362 g (32%). Anal. Calc. for $C_{19}H_{20}N_3O_{14}P_2Co_3$: C 30.30, H 2.68, N 5.58%. Found: C 30.27, H 3.07, N 5.54%. IR (KBr pellet, cm^{-1}): 3305m ($\nu_{O\text{-}H}$), 3084m, 2688w, 1589vs ($\nu_{as CO}$), 1533m, 1493w, 1417m, 1356w, 1227w, 1143s ($\nu_{P=O}$), 1039s ($\nu_{P\text{-}O}$), 966s ($\nu_{P\text{-}O}$), 850w, 806m, 752m, 690m, 634m, 611m, 515m, 478m.

X-Ray crystallography

X-Ray data for **1–2** were collected at 293(2) K on a Rigaku Mercury CCD/AFC diffractometer using graphite-monochromated Mo Kα radiation (λ(Mo-Kα) = 0.71073 Å). Data of **1–2** were reduced with CrystalClear v1.3. Their structures were solved by direct methods and refined by full-matrix least-squares techniques on F^2 using SHELXTL-97.[16] All non-hydrogen atoms were treated anisotropically. Positions of all hydrogen atoms in **1** were located from a difference Fourier map and assigned with fixed isotropic thermal parameters. Hydrogen atoms bound to carbon atoms (except for C24, C26 and C27) were generated geometrically, and no attempts were performed to locate other hydrogen atoms in **2**. The coordinated 4,4′-bipyridines in **2** were disordered over two sites. And owing to the isolated 4,4′-bipyridines in **2** exhibited extensive disorder, the pyridyl rings were refined as rigid hexagons of 1.39 Å sides. Crystallographic data for compounds **1–2** are summarized in Table 1. Selected bond lengths and angles for compounds **1** and **2** are listed in Table 2 and 3, respectively. CCDC 727228 (**1**) and 727229 (**2**).

Table 1 Crystallographic data for compounds **1** and **2**

Compound	**1**	**2**
Formula	$C_{19}H_{16}N_3O_{12}P_2Mn_3$	$C_{19}H_{20}N_3O_{14}P_2Co_3$
FW	705.11	753.11
Space group	*P*-1	*P*-1
a (Å)	8.652(3)	9.9725(11)
b (Å)	10.293(3)	10.5369(10)
c (Å)	14.164(4)	14.1184(16)
α (deg)	106.843(3)	90.477(4)
β (deg)	97.861(2)	109.924(4)
γ (deg)	100.576(3)	98.596(4)
V (Å^3)	1162.3(6)	1376.3(3)
Z	2	2
T (K)	293(2)	293(2)
Measured/unique/observed reflections	9018/5242/4164	10558/6190/5212
D_{calcd} (g cm^3)	2.015	1.817
μ (mm^{-1})	1.817	1.976
GOF on F^2	1.005	1.055
R_{int}	0.0176	0.0232
$R1^a$ [$I>2\sigma(I)$]	0.0300	0.0518
$wR2^b$ [all data]	0.0866	0.1502

$^a R1 = \Sigma(\|F_o\| - \|F_c\|)/\Sigma \|F_o\|$. $^b wR2 = \{\Sigma w [(F_o^2 - F_c^2)]/\Sigma w [(F^2{}_o)^2]\}^{0.5}$.

Results and discussion

Structural descriptions

The asymmetric unit of **1** includes three crystallographically independent Mn(II) ions, two L^{3-} anions, one coordinated 4,4′-bipy linker and half isolated 4,4′-bipy group. The Mn1(II) ion is surrounded by four L^{3-} anions into a distorted [$Mn1O_6$] octahedral coordination geometry (Fig. 1). On the basal plane of the [$Mn1O_6$] octahedron, two L^{3-} anions are chelated to Mn1(II) ion though two pairs of oxygen atoms (O1a/O5a and O7/O11) to form two Mn-O-C-C-P-O chelating rings. The coordination mode is the same as that of $NaM[O_3PCH(OH)CO_2]$ (M=Mn, Fe, Co, Zn).[13c] While the two polar sites are occupied by two other phosphonate oxygen atoms (O3 and O8). The Mn2(II) ion is surrounded by three L^{3-} anions and one 4,4′-bipy group, resulting in a distorted [$Mn2N_1O_5$] octahedral coordination geometry. It is attractive that one L^{3-} anion is chelated to the Mn2(II) ion *via* three oxygen atoms (O9, O10 and O12), which has not been reported in previous work.[13] The coordination environment of Mn3(II) ion is same to that of Mn2(II) ion. The Mn–O bond lengths are in the range of 2.0786(14)–2.4481(13) Å. On the other hand, the L^{3-} anion exhibits a new pentadentate mode to combine five Mn(II) ions (Scheme 1a).

The Mn2(II) and Mn3(II) ions are combined by two phosphonate oxygen atoms (O2,O9) into a binuclear unit. The angles of Mn2–O2–Mn3 and Mn2–O9–Mn3 are 100.28(5) and 99.82(5)°, respectively. And the Mn2···Mn3 distance is only 3.398 Å. The interactions between Mn1(II) and Mn2(II) ions through three

Table 2 Selected bond lengths (Å) and angles (°) for compound **1**

Mn(1)–O(1)^a	2.0898(14)	Mn(2)–O(10)	2.2544(14)
Mn(1)–O(3)	2.3492(13)	Mn(2)–O(12)	2.3003(14)
Mn(1)–O(5)^a	2.1661(14)	Mn(2)–N(1)	2.2464(17)
Mn(1)–O(7)	2.0786(14)	Mn(3)–O(2)	2.2739(13)
Mn(1)–O(8)	2.4481(13)	Mn(3)–O(3)	2.1462(13)
Mn(1)–O(11)	2.1807(14)	Mn(3)–O(4)	2.2505(14)
Mn(2)–O(2)	2.1520(13)	Mn(3)–O(6)	2.3091(13)
Mn(2)–O(8)^b	2.1405(13)	Mn(3)–O(9)	2.1485(13)
Mn(2)–O(9)	2.2918(13)	Mn(3)–N(2)	2.2423(17)
O(1)^a–Mn(1)–O(3)	95.36(5)	O(8)^b–Mn(2)–N(1)	93.73(6)
O(1)^a–Mn(1)–O(5)^a	91.33(5)	O(9)–Mn(2)–O(10)	77.41(5)
O(1)^a–Mn(1)–O(7)	175.30(4)	O(9)–Mn(2)–O(12)	86.13(5)
O(1)^a–Mn(1)–O(8)	82.70(5)	O(9)–Mn(2)–N(1)	165.52(5)
O(1)^a–Mn(1)–O(11)	87.53(5)	O(10)–Mn(2)–O(12)	67.86(5)
O(3)–Mn(1)–O(5)^a	96.46(5)	O(10)–Mn(2)–N(1)	89.31(6)
O(3)–Mn(1)–O(7)	88.30(5)	O(12)–Mn(2)–N(1)	83.49(6)
O(3)–Mn(1)–O(8)	176.17(4)	O(2)–Mn(3)–O(3)	97.25(5)
O(3)–Mn(1)–O(11)	85.00(5)	O(2)–Mn(3)–O(4)	77.85(5)
O(5)^a–Mn(1)–O(7)	91.19(5)	O(2)–Mn(3)–O(6)	85.95(5)
O(5)^a–Mn(1)–O(8)	86.89(5)	O(2)–Mn(3)–O(9)	80.18(5)
O(5)^a–Mn(1)–O(11)	178.23(4)	O(2)–Mn(3)–N(2)	169.94(5)
O(7)–Mn(1)–O(8)	93.48(5)	O(3)–Mn(3)–O(4)	109.82(5)
O(7)–Mn(1)–O(11)	89.85(5)	O(3)–Mn(3)–O(6)	175.66(4)
O(8)–Mn(1)–O(11)	91.61(5)	O(3)–Mn(3)–O(9)	104.39(5)
O(2)–Mn(2)–O(8)^b	101.39(5)	O(3)–Mn(3)–N(2)	91.20(6)
O(2)–Mn(2)–O(9)	79.70(5)	O(4)–Mn(3)–O(6)	67.89(5)
O(2)–Mn(2)–O(10)	140.06(5)	O(4)–Mn(3)–O(9)	141.17(5)
O(2)–Mn(2)–O(12)	78.38(5)	O(4)–Mn(3)–N(2)	94.17(6)
O(2)–Mn(2)–N(1)	107.91(6)	O(6)–Mn(3)–O(9)	79.01(5)
O(8)^b–Mn(2)–O(9)	96.83(5)	O(6)–Mn(3)–N(2)	85.35(6)
O(8)^b–Mn(2)–O(10)	113.43(5)	O(9)–Mn(3)–N(2)	103.06(6)
O(8)^b–Mn(2)–O(12)	176.95(5)		

Symmetry codes:^{a} –x + 1, –y + 1, –z + 1; ^{b} x + 1, y, z.

Table 3 Selected bond lengths (Å) and angles (°) for compound **2**

Co(1)–O(3)^c	2.070(3)	Co(2)–O(5)	2.140(3)
Co(1)–O(6)	2.257(3)	Co(2)–O(7)	2.014(3)
Co(1)–O(8)	2.074(3)	Co(2)–N(1)	2.121(4)
Co(1)–O(9)^b	2.067(3)	Co(3)–O(1)	2.063(3)
Co(1)–O(12)	2.144(3)	Co(3)–O(7)	2.252(3)
Co(1)–O(14)	2.103(3)	Co(3)–O(10)	2.138(3)
Co(2)–O(1)	2.303(3)	Co(3)–O(11)	2.091(3)
Co(2)–O(2)^a	2.022(3)	Co(3)–O(13)	2.036(3)
Co(2)–O(4)	2.153(3)	Co(3)–N(2)	2.142(3)
O(3)^c–Co(1)–O(6)	87.84(11)	O(2)^a–Co(2)–N(1)	92.45(13)
O(3)^c–Co(1)–O(8)	177.26(11)	O(4)–Co(2)–O(5)	73.78(10)
O(3)^c–Co(1)–O(9)^b	91.14(11)	O(4)–Co(2)–O(7)	153.58(11)
O(3)^c–Co(1)–O(12)	88.94(12)	O(4)–Co(2)–N(1)	97.35(13)
O(3)^c–Co(1)–O(14)	92.89(13)	O(5)–Co(2)–O(7)	87.92(11)
O(6)–Co(1)–O(8)	93.08(11)	O(5)–Co(2)–N(1)	88.17(13)
O(6)–Co(1)–O(9)^b	84.17(11)	O(7)–Co(2)–N(1)	101.01(13)
O(6)–Co(1)–O(12)	174.03(12)	O(1)–Co(3)–O(7)	80.59(10)
O(6)–Co(1)–O(14)	87.28(13)	O(1)–Co(3)–O(10)	158.98(11)
O(8)–Co(1)–O(9)^b	91.52(11)	O(1)–Co(3)–O(11)	93.17(11)
O(8)–Co(1)–O(12)	89.92(11)	O(1)–Co(3)–O(13)	100.51(12)
O(8)–Co(1)–O(14)	84.58(13)	O(1)–Co(3)–N(2)	95.71(13)
O(9)–Co(1)–O(12)	100.92(14)	O(7)–Co(3)–O(10)	80.92(10)
O(9)–Co(1)–O(14)	170.40(14)	O(7)–Co(3)–O(11)	86.16(10)
O(12)–Co(1)–O(14)	87.87(15)	O(7)–Co(3)–O(13)	94.90(12)
O(1)–Co(2)–O(2)^a	91.79(10)	O(7)–Co(3)–N(2)	173.97(13)
O(1)–Co(2)–O(4)	79.89(10)	O(10)–Co(3)–O(11)	75.68(11)
O(1)–Co(2)–O(5)	87.18(10)	O(10)–Co(3)–O(13)	90.95(11)
O(1)–Co(2)–O(7)	80.35(10)	O(10)–Co(3)–N(2)	101.82(13)
O(1)–Co(2)–N(1)	175.11(12)	O(11)–Co(3)–O(13)	166.27(12)
O(2)^a–Co(2)–O(4)	94.21(11)	O(11)–Co(3)–N(2)	89.31(13)
O(2)^a–Co(2)–O(5)	167.95(11)	O(13)–Co(3)–N(2)	90.44(14)
O(2)^a–Co(2)–O(7)	103.76(11)		

Symmetry codes:^{a} –x, –y, –z; ^{b} –x + 1, –y + 1, –z; ^{c} x + 1, y, z.

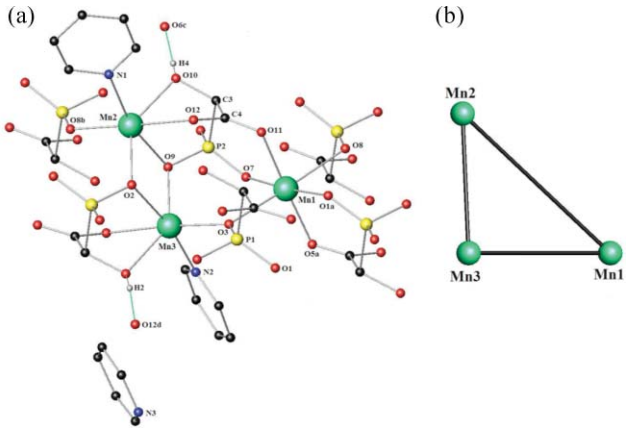

Fig. 1 (a) Ball-stick view of the coordinated environment of Mn(II) ions and (b) arrangement of the three Mn(II) ions in compound **1**. Green thin lines indicate hydrogen bondings. Symmetry codes for the generate atoms: *a* 1 – x, 1 – y, 1 – z; *b* 1 + x, y, z; *c* 2 – x, –y, 1 – z; *d* 2 – x, 1 – y, 1 – z.

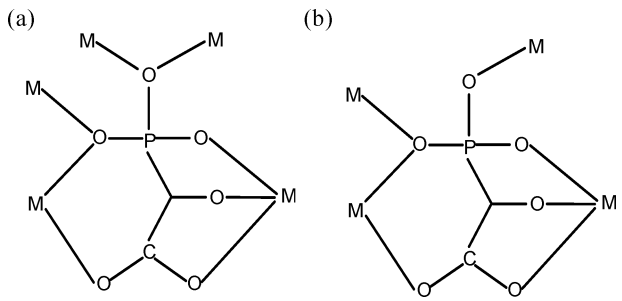

Scheme 1

bridge groups, including O9–P2–O7, O12–C4–O11, and O10–C3–C4–O11, resulting in the Mn1 ··· Mn2 distance is 5.276 Å. Besides the O9–P2–O7, the Mn1(II) ion interacts with the Mn3(II) ion also through a phosphonate oxygen atom (O3). The bond angle of Mn1–O3–Mn3 is 117.09(6)°, and the Mn1 ··· Mn3 distance is 3.997 Å. It is interesting that the three adjacent Mn(II) ions are arranged into an approximate right-angled triangle. The Mn1(II) ion and the binuclear unit connect each other alternatively into an infinite chain (Fig. 2). And the chains are bridged by -PO_3 groups to form a hybrid layer. Within the layer, hydrogen bondings appear between the hydroxyl and the carboxylate groups

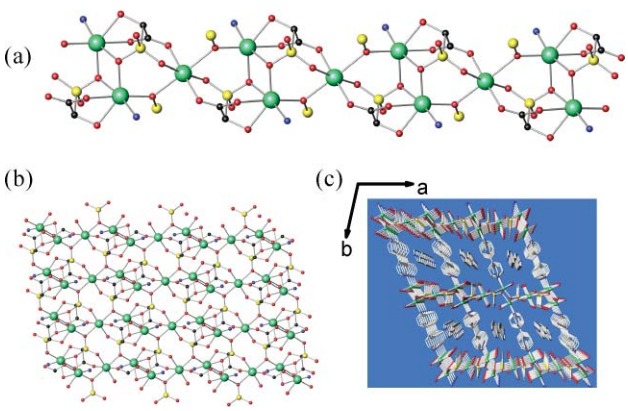

Fig. 2 Ball-stick representations of (a) the chain, (b) the layer, and (c) the 3D framework in compound **1**.

(O4 · · · O12d) and (O10 · · · O6c). The hybrid layers are further pillared by the coordinated 4.4′-bipy groups into a 3D neutral framework containing 1D parallelogram-shaped channels with approximate sizes of 9×11 Å^2 along the *b* axis. And the channel is occupied by isolated 4.4′-bipy groups. In addition, a Mn–O chain is hidden among the above mentioned chain. The Mn–O chain is similar to the Co–O chain of $[Co_3(OH)_2(btca)_2]\cdot 3.7H_2O$ (H_2bcta = benzotriazole-5-carboxylic acid).[17] However, the Co–O chain is interrupted by btca groups to form a sheet. While, the Mn–O chain is further bridged by O–P–O groups into a sheet.

The asymmetric unit of **2** also includes three crystallographically independent Co(II) ions, two L^{3-} anions, one coordinated 4,4′-bipy linker, half isolated 4,4′-bipy group, as well as two coordinated water molecules. The presence of water molecules are verified by the IR spectrum, which displays a broad absorption band in the range of 3050–3400 cm^{-1} corresponding to the O–H stretching vibration of water. As shown in Fig. 3, the Co1(II) ion has a distorted [Co1O$_6$] octahedron coordination geometry and is ligated by five oxygen atoms from three L^{3-} anions and one coordinated water molecule. On the basal plane of the [Co1O$_6$] octahedron, two L^{3-} anions are chelated to Co1(II) ion though two pairs of oxygen atoms (O3c/O6 and O8/O12) to form two Co-O-C-C-P-O chelating rings. This is the same as that of Mn1(II) in **1**. While the two polar sites are occupied by one phosphonate oxygen atom (O9b) and one coordinated water molecule (O14), respectively. Similar to that of Mn2(II) ion in **1**, the Co2(II) ion is surrounded by three L^{3-} anions and one coordinated 4,4′-bipy group, resulting in a distorted [Co2N$_1$O$_5$] octahedral coordination geometry. And one L^{3-} anion is also chelated to Co2(II) ion through three oxygen atoms (O1, O4 and O5). The coordination environment of Co3(II) ion is similar to that of Co2(II) ion, except that one L^{3-} anion is replaced by one coordinated water molecule (O13). The Co–O bond lengths are in the range of 2.014(3)–2.303(3) Å. Due to the two water molecules taking part in coordination with Co(II) ions and occupying two sites, the L^{3-} anion only bridges four Co(II) ions in a new tetradentate mode, which is different from that in **1** (Scheme 1b).

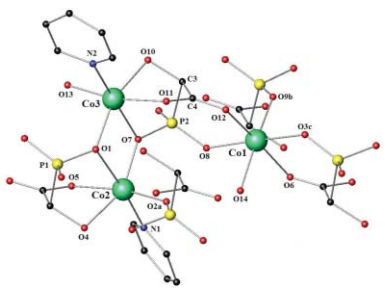

Fig. 3 Ball-stick view of the coordinated environment of Co(II) ions in compound **2**. Symmetry codes for the generate atoms: *a* –x, –y, –z; *b* 1 – x, 1 – y, –z; *c* 1 + x, y, z.

Similar to that in **1**, the Co2(II) and Co3(II) ions are combined by two phosphonate oxygen aoms (O1,O7) into a binuclear unit. The angles of Co2–O1–Co3 and Co2–O7–Co3 are 97.92(10) and 101.07(11)°, respectively. And the Co2 · · · Co3 distance is only 3.297 Å, which is slightly shorter than that of Mn2 · · · Mn3. The interaction between Co1(II) and Co2(II) ions through an O7–P2–O8 group, results in the Co1 · · · Co2 distance of 5.032 Å. Besides the O7–P2–O8 group, the Co1(II) ion interacts with the Co3(II) ion also through O11–C4–O12, and O10–C3–C4–O12 groups. As a result, the Co1 · · · Co3 distance is 5.394 Å, which is obviously longer than that of Mn1 · · · Mn3. The three Co(II) ions are arranged into a triangle. The Co1(II) ion and the binuclear unit connect to each other alternatively to form an infinite chain. And the chains are also bridged by -PO_3 groups into a hybrid layer (Fig. 4). The hybrid layers are further pillared by the coordinated 4.4′-bipy groups into a 3D neutral framework possessing 1D parallelogram-shaped channels with approximate sizes 9×11 Å^2 along the *b* axis. And the channel is occupied by an isolated 4,4′-bipy group. Different from the Mn–O chain in **1**, no Co–O chain is found in **2**.

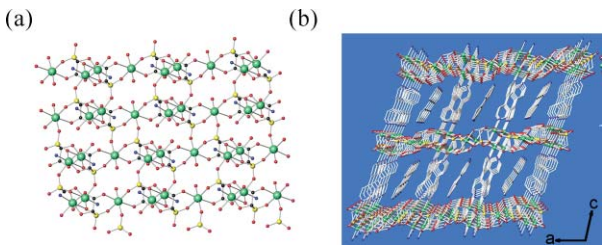

Fig. 4 Ball-stick representations of (a) the layer and (b) the 3D framework in compound **2**.

Clearly, after 4,4′-bipyridine was introduced as a second ligand into metal 2-hydroxyl(phosphono)acetate, the pillared framework of compounds **1** and **2** are remarkably different from the layered $M(HO_3PCH(OH)CO_2)(H_2O)_2$ and the condensed $NaM(O_3PCH(OH)CO_2)$ (M = Mn, Co).[13a,c] This is due to 4,4′-bipyridine being a linear ligand, which can act as rigid pillars between adjacent hybrid layers. And 4,4′-bipyridine can also serve as a guest occupying the void between adjacent layers to direct the channels and maintain the pillared framework.

Thermal stability

Thermogravimetric analysis (TGA) illustrates that under an air atmosphere there is a little weight loss up to 320 °C for compound **1**. Upon further heating, an abrupt weight loss stage appears due to the decomposition of the L^{3-} anion and 4,4′-bipy ligands, resulting in the collapse of the 3D framework. In addition, after as-prepared **1** was annealed at 300 °C under an air atmosphere for two hours and cooled to room temperature, the powder XRD patterns are all essentially in agreement with those simulated from single-crystal XRD data, which unambiguously indicates little change in the framework. TGA of compound **2** illustrates that under nitrogen gas flow there is a weight loss stage between 120 and 170 °C with 5.07% weight loss, corresponding to the loss of two coordinated water molecules (calculated 4.78%). Then an abrupt weight loss stage starts from 330 °C, due to the decomposition of the L^{3-} anion and 4,4′-bipy ligands. Furthermore, after as-prepared **2** was annealed at 170 °C under an air atmosphere for two hours and cooled to room temperature, the powder XRD patterns are in agreement with those of as-prepared **2** except that (001) and (002) peaks shift slightly to the higher diffraction angles. This indicates that the framework is contracted slightly.

Luminescent properties

Solid-state luminescent properties of solids **1–2** were investigated under ambient temperature. No luminescent emission for solid **2** can be detected under our experimental conditions. This may be due to self-absorption through the d–d transition of the Co(II) ion in the range of 428–654 nm.[13c] In contrast, solid **1** displays purple-blue luminescence with maximum and shoulder bands at 430 and 408 nm, respectively (Fig. 5). The purple-blue emission profile is close to that of 4,4′-bipyridine. Since Mn(II) ion is an important luminescent activator in many red phosphors, the purple-blue emission can not be attributed to LMCT (ligand-to-metal charge transfer).[18] In addition, no luminescent emission for $[Mn(HO_3PCH(OH)CO_2)]$ can be detected under our experimental conditions in spite of the bright blue-green luminescence of $H_2O_3PCH(OH)CO_2H$ solution.[13a] From above results, it seems that the purple-blue emission of solid **1** may be assigned to the ligand-centered π–π* transition of 4,4′-bipyridine.

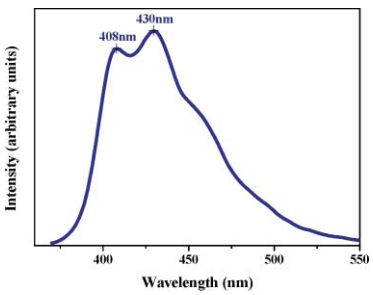

Fig. 5 Normalized fluorescent emission spectrum of compound **1**.

Magnetic properties

The temperature dependence of the magnetic susceptibility for compounds **1** and **2** from 2 K to room temperature under an applied field of 5 kOe were studied with a Quantum Design PPMS model 6000 magnetometer. For solid **1**, the observed $\chi_m T$ value per Mn_3 unit at 309 K is 12.15 cm^3 K mol^{-1}. By using the equation $\mu_{eff} = (8\chi_m T)^{1/2}$, the average effective magnetic moment of 5.69 μ_B per manganese atom at 309 K is consistent with the expected spin-only value of 5.92 μ_B ($g = 2$, $s = 5/2$), and also according to the reported magnetic moments of Mn(II) in the range of 5.2–5.9 μ_B.[19] Upon cooling, the $\chi_m T$ decreases continuously and reaches a minimum value of 7.57 cm^3 K mol^{-1} at 20 K (Fig. 6), indicating a dominant antiferromagnetic (AF) interaction In the temperature range of 20–309 K, the magnetic susceptibility follows the Curie–Weiss law [$\chi_m^{-1} = 1.32(1) + 0.07805(6)\ T$] ($r = 0.9999$), with a Curie constant of 12.81 cm^3 K mol^{-1} and a Weiss constant of −16.9 K. The field-cooled susceptibility curve is the same as that of the zero-field cooled, revealing that the antiferromagnetic ordering appears at low temperature and low field ($H_{meas.} = 100$ Oe, $T_N = 9.0$ K). And the field dependent magnetization measured at 2 K shows an overall S-shaped curve. These results suggest that solid **1** is characteristic of metamagnetism, which is similar to those of pillared cobalt phosphates and a few metal phosphonates.[17,20,21]

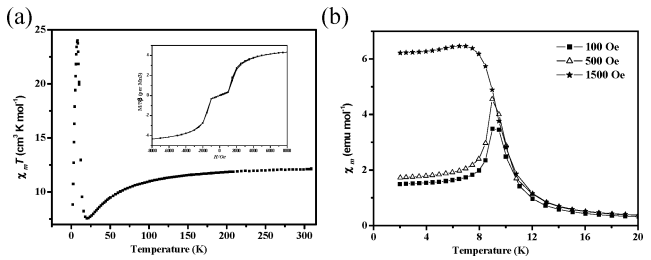

Fig. 6 (a) The $\chi_m T$ *versus* T curve and (b) temperature dependence of the field-cooled magnetic susceptibility per Mn_3 unit in compound **1**. Inset: field dependence of magnetization at 2 K.

The angles Mn2–O2–Mn3 (100.28(5)°) and Mn2–O9–Mn3 (99.82(5)°) and the Mn2···Mn3 distance (3.398 Å) are close to those in the compound $Mn_2\{[(C_7H_5N_2)CH_2]_2NCH_2PO_3\}_2(H_2O)_2{\cdot}2H_2O$, which shows a ferromagnetic exchange between the Mn(II) ions.[11b] So in solid **1**, the angles Mn2–O2–Mn3 and Mn2–O9–Mn3 are expected to show a ferromagnetic exchange interaction. Since the magnetization *vs* field curve at 2 K shows no hysteresis at very low fields and the negative value of the Weiss constant, antiferromagnetic interactions tend to dominate in the competitive environment.

It is worth noting that the metamagnetism of solid **1** is obviously different from the antiferromagnetism of $Mn(HO_3PCH(OH)CO_2)(H_2O)_2$ and $NaMn(O_3PCH(OH)CO_2)$.[13a,c] This is also attributed to 4,4′-bipyridine for three reasons. Firstly, 4,4′-bipyridine takes part in coordination with Mn(II) ion and occupies two sites, which can promote 2-hydroxyl(phosphono)-acetate to bridge more metal ions around itself. As a result, the distances of Mn(II) ions are obviously shortened, which may enhance the ferromagnetic interactions. Secondly, 4,4′-bipyridine acts as a rigid pillar to increase the separated distance of adjacent hybrid layers. This can prevent interlayer antiferromagnetic exchange.[17] Finally, 4,4′-bipyridine serves as a guest lying in the void between adjacent layers to weaken interlayer antiferromagnetic exchange.

For solid **2**, the $\chi_m T$ value is 8.78 cm^3 K mol^{-1} at 310 K, and it decreases continuously with decreasing temperature down to a minimum value of 3.97 cm^3 K mol^{-1} at 9.5 K (Fig. 7). By using the equation $\mu_{eff} = (8\chi_m T)^{1/2}$, the average effective cobalt moment of 4.84 μ_B per cobalt atom at 310 K is obviously higher than the reported spin-only value of 3.87 μ_B and is in the range of 4.4–5.2 μ_B due to the orbital contribution at room temperature. Upon further cooling, the $\chi_m T$ value increases rapidly to a maximum of 5.18 cm^3 K mol^{-1} at 4 K, and then decreases to 3.89 cm^3 K mol^{-1} at 2 K. The behavior of $\chi_m T$ below 9.5 K is different from those of $Co(HO_3PCH(OH)CO_2)(7H_2O)_2$ and $NaCo(O_3PCH(OH)CO_2)$.[13a,c] In the temperature range of 2–308 K, the magnetic susceptibility follows the Curie–Weiss law [$\chi_m^{-1} = 1.73(8) + 0.1097(5)$ T] ($r = 0.9998$), with a Curie constant of 9.12 cm^3 K mol^{-1} and a Weiss constant of −15.8 K. These results indicates mainly antiferromagnetic interaction of Co(II) ions.

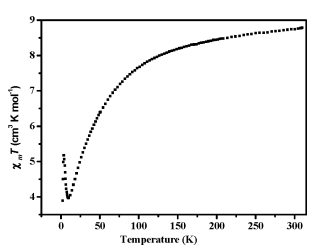

Fig. 7 The $\chi_m T$ *versus* T curve per Co_3 unit in compound **2**.

Conclusions

We have described the syntheses and crystal structures of two new metal phosphonates, $[Mn_3(4,4'\text{-bipy})(O_3PCH(OH)\ CO_2)_2]\cdot(4,4'\text{-bipy})_{0.5}$ (**1**) and $[Co_3(4,4'\text{-bipy})(H_2O)_2(O_3PCH\ (OH)CO_2)_2]\cdot(4,4'\text{-bipy})_{0.5}$ (**2**). Both are 3D pillared structures in which the inorganic–organic hydrid layers made up of $[MO_6]$ and $[MNO_5]$ (M = Mn, Co) octahedra are bridged by 2-hydroxyl(phosphono)acetate through -OH, -COO and $-PO_3$ groups. The 4,4′-bipys serve as rigid pillars and guests to separate adjacent layers and form 1D parallelogram-shaped channels with approximate sizes 9×11 Å^2. Solid **1** is thermally stable up to 300 °C under an air atmosphere and displays a purple-blue luminescence. The results of magnetic measurement indicate solid **1** exhibits metamagnetism. Future efforts are focused on selecting other interesting secondary ligands to expand metal phosphonates and investigate the relationship between structure and magnetic properties.

Acknowledgements

This research was supported by grants from the State Key Laboratory of Structure Chemistry, Fujian Institute of Research on the Structure of Matter, Chinese Academy of Sciences (CAS), the National Ministry of Science and Technology of China (2007CB815301 and 2006CB932900), the National Science Foundation of China (20733003, 20801055 and 20673118), the Science Foundation of CAS and Fujian Province for research funding support (KJCX2-YW-M05 and 2007J0171).

Notes and references

1 A. Clearfield, Metal phosphonate chemistry in *Progress in Inorganic Chemistry*, *Vol. 47* (Ed.: K. D. Karlin), Wiley, New York, 1998, pp. 371-511.
2 (*a*) J. G. Mao, *Coord. Chem. Rev.*, 2007, **251**, 1493; (*b*) E. Matczak-Jon and V. Vienova-Adrabińska, *Coord. Chem. Rev.*, 2005, **249**, 2458; (*c*) K. Maeda, *Microporous Mesoporous Mater.*, 2004, **73**, 47.
3 T. H. Bray, A. G. D. Nelson, G. B. Jin, R. G. Haire and T. E. Albrecht-Schmitt, *Inorg. Chem.*, 2007, **46**, 10959.
4 (*a*) C. Serre, J. A. Groves, P. Lightfoot, A. M. Z. Slawin, P. A. Wright, N. Stock, T. Bein, M. Haouas, F. Taulelle and G. Férey, *Chem. Mater.*, 2006, **18**, 1451; (*b*) R. B. Fu, X. H. Huang, S. M. Hu, S. C. Xiang and X. T. Wu, *Inorg. Chem.*, 2006, **45**, 5254; (*c*) R. B. Fu, S. M. Hu and X. T. Wu, *Cryst. Growth Des.*, 2007, **7**, 1134.
5 (*a*) Q. Yue, J. Yang, G. H. Li, G. D. Li and J. S. Chen, *Inorg. Chem.*, 2006, **45**, 4431; (*b*) X. Shi, G. S. Zhu, S. L. Qiu, K. L. Huang, J. H. Yu and R. R. Xu, *Angew. Chem., Int. Ed.*, 2004, **43**, 6482; (*c*) X. G. Liu, S. S. Bao, Y. Z. Li and L. M. Zheng, *Inorg. Chem.*, 2008, **47**, 5525.
6 (*a*) O. Oms, J. L. Bideau, F. Leroux, A. von der Lee, D. Leclercq and A. Vioux, *J. Am. Chem. Soc.*, 2004, **126**, 12090; (*b*) J. Wu, Y. L. Song, E. P. Zhang, H. W. Hou, Y. T. Fan and Y. Zhu, *Chem.–Eur. J.*, 2006, **12**, 5823.
7 (*a*) V. Baskar, M. Shanmugam, E. C. Sañudo, M. Shanmugam, D. Collison, E. J. L. McInnes, Q. Wei and R. E. P. Winpenny, *Chem. Commun.*, 2007, 37; (*b*) S. Konar, N. Bhuvanesh and A. Clearfield, *J. Am. Chem. Soc.*, 2006, **128**, 9604.
8 (*a*) L. M. Zheng, S. Gao, P. Yin and X. Q. Xin, *Inorg. Chem.*, 2004, **43**, 2151; (*b*) D. Kong, Y. Li, X. Ouyang, A. V. Prosvirin, H. Zhao, Jr., J. H. Ross, K. R. Dunbar and A. Clearfield, *Chem. Mater.*, 2004, **16**, 3020; (*c*) X. M. Zhang, *Eur. J. Inorg. Chem.*, 2004, 544.
9 (*a*) S. Bauer, H. Mu1ller, T. Bein and N. Stock, *Inorg. Chem.*, 2005, **44**, 9464; (*b*) B. P. Yang and J. G. Mao, *Inorg. Chem.*, 2005, **44**, 566; (*c*) D. K. Cao, Y. Z. Li, Y. Song and L. M. Zheng, *Inorg. Chem.*, 2005, **44**, 3599; (*d*) X. Y. Yi, B. Liu, R. Jiménez-Aparicio, F. A. Urbanos, S. Gao, W. Xu, J. S. Chen, Y. Song and L. M. Zheng, *Inorg. Chem.*, 2005, **44**, 4309; (*e*) B. Liu, Y. Z. Li and L. M. Zheng, *Inorg. Chem.*, 2005, **44**, 6921; (*f*) J. L. Song and J. G. Mao, *Chem.–Eur. J.*, 2005, **11**, 1417; (*g*) P. Yin, S. Gao, Z. M. Wang, C. H. Yan, L. M. Zheng and X. Q. Xin, *Inorg. Chem.*, 2005, **44**, 2761.
10 (*a*) S. S. Bao, G. S. Chen, Y. Wang, Y. Z. Li, L. M. Zheng and Q. H. Luo, *Inorg. Chem.*, 2006, **45**, 1124; (*b*) D. Cave, F. C. Coomer, E. Molinos, H. H. Klauss and P. T. Wood, *Angew. Chem., Int. Ed.*, 2006, **45**, 803; (*c*) J. A. Groves, S. R. Miller, S. J. Warrender, C. Mellot-Draznieks, P. Lightfoota and P. A. Wright, *Chem. Commun.*, 2006, 3305; (*d*) S. F. Tang, J. L. Song, X. L. Li and J. G. Mao, *Cryst. Growth Des.*, 2006, **6**, 2322; (*e*) D. K. Cao, J. Xiao, Y. Z. Li, J. M. Clemente-Juan, E. Coronado and L. M. Zheng, *Eur. J. Inorg. Chem.*, 2006, 1830; (*f*) B. Liu, P. Yin, X. Y. Yi, S. Gao and L. M. Zheng, *Inorg. Chem.*, 2006, **45**, 4205.
11 (*a*) S. F. Tang, J. L. Song, X. L. Li and J. G. Mao, *Cryst. Growth Des.*, 2007, **7**, 360; (*b*) D. K. Cao, J. Xiao, J. W. Tong, Y. Z. Li and L. M. Zheng, *Inorg. Chem.*, 2007, **46**, 428; (*c*) J. M. Liang and G. K. H. Shimizu, *Inorg. Chem.*, 2007, **46**, 10449; (*d*) D. K. Cao, Y. Z. Li and L. M. Zheng, *Inorg. Chem.*, 2007, **46**, 7571; (*e*) B. Liu, B. L. Li, Y. Z. Li, Y. Chen, S. S. Bao and L. M. Zheng, *Inorg. Chem.*, 2007, **46**, 8524; (*f*) S. Bauer, J. Marrot, T. Devic, G. Férey and N. Stock, *Inorg. Chem.*, 2007, **46**, 9998.
12 (*a*) B. P. Yang, A. V. Prosvirin, Y. Q. Guo and J. G. Mao, *Inorg. Chem.*, 2008, **47**, 1453; (*b*) Y. F. Yang, Y. S. Ma, L. R. Guo and L. M. Zheng, *Cryst. Growth Des.*, 2008, **8**, 1213; (*c*) A. N. Alsobrook, W. Zhan and T. E. Albrecht-Schmitt, *Inorg. Chem.*, 2008, **47**, 5177.
13 (*a*) R. B. Fu, S. C. Xiang, H. S. Zhang, J. J. Zhang and X. T. Wu, *Cryst. Growth Des.*, 2005, **5**, 1795; (*b*) R. B. Fu, H. S. Zhang, L. S. Wang, S. M. Hu, Y. M. Li, X. H. Huang and X. T. Wu, *Eur. J. Inorg. Chem.*, 2005, 3211; (*c*) Z. Z. Lai, R. B. Fu, S. M. Hu and X. T. Wu, *Eur. J. Inorg. Chem.*, 2007, 5439.
14 (*a*) J. L. Song, H. H. Zhao, J. G. Mao and K. R. Dunbar, *Chem. Mater.*, 2004, **16**, 1884; (*b*) R. Pothiraja, M. Sathiyendiran, R. J. Butcher and R. Murugavel, *Inorg. Chem.*, 2004, **43**, 7585; (*c*) C. H. Lin and K. H. Lii, *Inorg. Chem.*, 2004, **43**, 6403; (*d*) S. M. Ying and J. G. Mao, *Eur. J. Inorg. Chem.*, 2004, 1270; (*e*) K. J. Lin, S. J. Fu, C. Y. Cheng, W. H. Chen and H. M. Kao, *Angew. Chem., Int. Ed.*, 2004, **43**, 4186; (*f*) J. L. Song, C. Lei and J. G. Mao, *Inorg. Chem.*, 2004, **43**, 5630.
15 (*a*) D. Y. Kong, J. Zoñ, J. McBee and A. Clearfield, *Inorg. Chem.*, 2006, **45**, 977; (*b*) S. M. Ying and J. G. Mao, *Cryst. Growth Des.*, 2006, **6**, 964; (*c*) R. Murugavel and S. Shanmugan, *Dalton Trans.*, 2008, 5358.
16 G. M. Sheldrick, *SHELXT 97, Program for Crystal Structure Refinement*, University of Göttingen, Germany, 1997.
17 X. M. Zhang, Z. M. Hao, W. X. Zhang and X. M. Chen, *Angew. Chem., Int. Ed.*, 2007, **46**, 3456–3459.
18 (*a*) Y. B. Dong, G. X. Jin, M. D. Smith, R. Q. Huang, B. Tang and H. C. zur Loye, *Inorg. Chem.*, 2002, **41**, 4909; (*b*) X. D. Guo, G. S. Zhu, Q. R. Fang, M. Xue, G. Tian, J. Y. Sun, X. T. Li and S. L. Qiu, *Inorg. Chem.*, 2005, **44**, 3850; (*c*) J. Tao, M. L. Tong, J. X. Shi, X. M. Chen and S. W. Ng, *Chem. Commun.*, 2000, 2043; (*d*) M. García-Hipólito, Q. Alvarez-Fregoso, E. Martínez, C. Falcony and M. A. Aguilar-Frutis, *Opt. Mater.*, 2002, **20**, 113; (*e*) J. Wang, S. B. Wang and Q. Su, *J. Mater. Chem.*, 2004, **14**, 2569.
19 (*a*) F. Sanz, C. Parada, J. M. Rojo and C. Ruiz-Valero, *Chem. Mater.*, 2001, **13**, 1334; (*b*) R. l. Carlin, *Magneto-chemistry*, Springer-Verlag: New York, 1986.
20 (*a*) M. P. Shores, B. M. Bartlett and D. G. Nocera, *J. Am. Chem. Soc.*, 2005, **127**, 17986; (*b*) W. K. Chang, R. K. Chiang, Y. C. Jiang, S. L. Wang, S. F. Lee and K. H. lii, *Inorg. Chem.*, 2004, **43**, 2564; (*c*) X. Y. Wang, L. Wang, Z. M. Wang, G. Su and S. Gao, *Chem. Mater.*, 2005, **17**, 6369; (*d*) H. Z. Kou, S. Gao, B. W. Sun and J. Zhang, *Chem. Mater.*, 2001, **13**, 1431; (*e*) D. F. Li, L. M. Zheng, X. Y. Wang, J. Huang, S. Gao and W. X. Tang, *Chem. Mater.*, 2003, **15**, 2094; (*f*) T. F. Liu, H. L. Sun, S. Gao, S. W. Zhang and T. C. Lau, *Inorg. Chem.*, 2003, **42**, 4792.
21 (*a*) S. Z. Hou, D. K. Cao, X. G. Liu, Y. Z. Li and L. M. Zheng, *Dalton Trans.*, 2009, 2746; (*b*) P. Yin, S. Gao, L. M. Zheng, Z. M. Wang and X. Q. Xin, *Chem. Commun.*, 2003, 1076; (*c*) P. Yin, L. M. Zheng and X. Q. Xin, *Chem. Commun.*, 2001, 2346; (*d*) L. M. Zheng, S. Gao, H. H. Song, S. Decurtins, A. J. Jacobson and X. Q. Xin, *Chem. Mater.*, 2002, **14**, 3143; (*e*) M. Riou-Cavellec, M. Sanselme, M. Nogues, J. M. Grenèche and G. Férey, *Solid State Sci.*, 2002, **4**, 619.

